processes

MDPI

Article

Combustion Reaction Investigation of Marine Engine Mixed Fuel of Methane/Ammonia/Diesel

Jingmin Rui [1], Haibin Li [1], Jing Zhao [1], Xiuyuan Bai [1], Ce Zhang [1], Zhongjie Shi [2,3,*], Dehai Li [4], Junpeng Xin [5], Dongsheng Dong [6] and Longlong Jiang [7,*]

1 School of Automotive Engineering, Tianjin Vocational Institute, Tianjin 300410, China; 220018@tjtc.edu.cn (J.R.)
2 School of Mechanical Engineering, Beijing Institute of Technology, Beijing 100081, China
3 Hefei Institute of Unmanned Intelligent Equipment, Beijing Institute of Technology, Hefei 230600, China
4 Tianjin Linghai Weiye Technology Development Co., Ltd., Tianjin 300300, China
5 Jinyang Automotive Technology (Tianjin) Co., Ltd., Tianjin 300300, China
6 School of Naval Architecture, Ocean and Energy Power Engineering, Wuhan University of Technology, Wuhan 430063, China
7 College of Mechanical and Electrical Engineering, Dalian Minzu University, Dalian 116600, China
* Correspondence: shizhongjie@bit.edu.cn (Z.S.); 20251637@dlnu.edu.cn (L.J.)

Abstract

The utilization of low- and zero-carbon fuels in internal combustion engines is gaining increasing interest. In marine engine applications, the co-combustion of methane and ammonia has emerged as a promising strategy for reducing carbon emissions. In this work, a chemical kinetic mechanism for n-heptane/methane/ammonia blended fuel was developed and validated. Using this mechanism, sensitivity and chemical kinetic analyses were performed to explore the ignition characteristics of the fuel mixture. The results indicate that at an initial temperature of 1000 K, reaction R152 ($C_7H_{15\text{-}2} = CH_3 + C_6H_{12}$) exerts the strongest inhibiting effect on ignition. $C_7H_{15\text{-}2}$ is a major low-reactivity intermediate generated during n-heptane decomposition, and the accumulation of such intermediates contributes to the negative temperature coefficient (NTC) behavior. A cross-reaction between CH_4 and NH_3, R111 ($CH_4 + NH_2 = CH_3 + NH_3$), was identified, which impedes the smooth progression of oxidation. Elevated temperatures, oxygen-rich conditions, and higher ammonia blending ratios promote the formation of NO. The production of N_2O is primarily governed by reaction R105 ($NH + NO = N_2O + H$), whose rate increases with the NH_3 molar fraction. Consumption of N_2O occurs mainly via reactions R92 ($N_2O + H = N_2 + OH$) and R94 (N_2O (+M) = N_2 + O (+M)), both of which occur later than its formation through R105, indicating that N_2O consumption is more sensitive to temperature.

Keywords: marine engine; combustion reaction; n-heptane/methane/ammonia mechanism; chemical kinetic analysis; ignition delay time; reducing carbon emissions

Check for updates

Academic Editor: Cherng-Yuan Lin

Received: 19 November 2025
Revised: 12 December 2025
Accepted: 12 January 2026
Published: 28 January 2026

Correction Statement: This article has been republished with a minor change. The change does not affect the scientific content of the article and further details are available within the backmatter of the website version of this article.

Copyright: © 2026 by the authors. Licensee MDPI, Basel, Switzerland. This article is an open access article distributed under the terms and conditions of the Creative Commons Attribution (CC BY) license.

1. Introduction

In recent years, hydrogen and ammonia have emerged as promising zero-carbon fuels for internal combustion engines. However, their distinct heating values and combustion properties introduce challenges to the conventional thermodynamic cycle, including unstable ignition, incomplete combustion, and increased NO_x formation. These issues highlight the need for further research on optimized combustion strategies tailored to alternative fuels. Due to its physical properties, the use of hydrogen alone has several disadvantages:

hydrogen is the lightest element with an extremely low volumetric energy density, and it also poses safety concerns (flammable and forms explosive mixtures with air). In addition, hydrogen has high logistical costs, and currently, hydrogen refueling stations are scarce. Therefore, the only feasible solution is to store compressed gaseous hydrogen (CGH_2) in pressurized tanks, with the main tank pressure at 350 or 700 bar and the fixed tank pressure at 120 bar [1,2]. Although CGH_2 has moderate energy density, high pressure, and excellent flammability, it also presents safety risks. Of course, hydrogen can be stored in liquid form (LH_2); however, liquefying hydrogen consumes a large amount of energy (up to 30% of its lower heating value) and leads to evaporation losses [3]. Ammonia, as an excellent hydrogen carrier, provides the same clean energy advantages as hydrogen while also offering the additional benefits of mature production, storage, and transportation infrastructure [4]. Ammonia, as a carbon-free fuel, has an ignition point of 650 °C. Compared to hydrogen, ammonia has a lower risk of fire and is less likely to explode. When used as an internal combustion engine fuel, it is less prone to knocking, backfiring, or other abnormal combustion phenomena. The global push toward carbon neutrality has made ammonia an increasingly attractive alternative fuel for engines, which is also a key focus of current internal combustion engine research. For many years, scholars both domestically and internationally have conducted extensive research on ammonia's basic flame characteristics, combustion enhancement methods, chemical kinetic mechanisms, and the combustion characteristics and performance of ammonia-fueled engines [5–8], in order to explore feasible ways to achieve stable and efficient combustion in ammonia-fueled engines. A summary of representative chemical kinetic mechanisms for ammonia combustion is presented in Table 1.

Table 1. A brief overview of the chemical reaction kinetics mechanism involving ammonia as a fuel.

Mechanism Model	Fuel	Species/Reactions	Parameters for Validation
Mathieu and Petersen (2015) [9]	NH_3/CH_4	54/278	Ignition delay
Song (2016) [10]	NH_3	32/204	-
Nakamura (2017) [11]	NH_3	38/232	Species concentration
Glarborg (2018) [12]	NH_3/C1-C2	151/1397	Species concentration/Ignition delay
Shrestha (2018) [13]	NH_3	125/1090	Laminar flame speed/Species concentration/Ignition delay
Otomo (2018) [14]	NH_3	32/213	Laminar flame speed
Okafor (2019) [15]	NH_3/CH_4	43/130	Laminar flame speed/Species concentration
Mei (2019) [16]	NH_3	38/265	Laminar flame speed
Li (2019) [17]	$NH_3/H_2/CH_4$	128/957	Laminar flame speed/Ignition delay
Stagni (2022) [18]	NH_3	31/203	Laminar flame speed/Ignition delay
Han (2020) [19]	NH_3/H_2/Syngas	35/174	Laminar flame speed
Yu (2020) [20]	NH_3/N-C_7H_{16}	1376/6499	Ignition delay
Wang (2021) [21]	$NH_3/CH_3OH/C_2H_5OH$	91/444	Laminar flame speed
Bertolino (2021) [22]	NH_3	31/230	Laminar flame speed/Species concentration/Ignition delay
Sun (2022) [23]	NH_3/CH_4	66/486	Laminar flame speed/Ignition delay
Liao (2023) [24,25]	$NH_3/H_2/CH_4$	178/1364	Ignition delay
Xu (2023) [26]	NH_3/N-C_7H_{16}	69/389	Laminar flame speed/Species concentration/Ignition delay
Wu (2023) [27]	$C_{10}H_{22}/C_8H_{18}/C_7H_{14}/C_7H_8/NH_3$	124/660	Laminar flame speed/Ignition delay
Wang (2023) [28]	NH_3/N-C_7H_{16}	74/495	Laminar flame speed/Ignition delay

An overview of the chemical reaction kinetics mechanisms involving ammonia fuels is shown in Table 1. Researchers have proposed many detailed chemical reaction models for ammonia or ammonia/hydrocarbon mixtures. Otomo et al. [14] compared the predicted results of several ammonia models with experimental data from the literature and found that the models previously proposed by Dagaut et al. [29], Mathieu et al. [9], Klippenstein et al. [30], Tian et al. [31], and Song et al. [10] significantly overestimated the laminar flame speed. As a result, Otomo et al. [14] proposed an improved ammonia oxidation mechanism based on Song's model [10], which showed good performance in ignition delay and laminar flame speed. However, the improved ammonia mechanism by Otomo et al. is only applicable to ammonia/air and ammonia/hydrogen/air combustion, and does not apply to ammonia/methane mixtures. Shrestha et al. [13] proposed a detailed H_2–CO–CH_4–NO–NH_3 mechanism and validated it using ignition delay, laminar flame speed, and species concentration data. However, some NH_3-C1 species and reactions are still missing in Shrestha's mechanism. Bertolino et al. [22] optimized the ammonia mechanism by Stagni et al. [18] using evolutionary and data-driven methods. The mechanism was optimized through a database containing 635 ammonia combustion experimental data points, covering standard targets such as ignition delay time (IDTs), species distribution, and laminar burning velocity (LBV). The final optimized mechanism showed satisfactory agreement with experimental results across the entire range of operating conditions. As shown in Table 1, in recent years, there has been an increasing amount of research on the reaction mechanisms of ammonia with other carbon-containing fuels. Mixing ammonia with other carbon-based fuels not only improves the combustion efficiency of ammonia fuels but also reduces carbon emissions, providing a technical approach to solve the current issue of slow combustion speed of ammonia fuels.

The ignition process of alternative fuels is crucial for subsequent combustion processes and emission control. The combustion chemical reactions in internal combustion engines are actually driven by numerous elementary reactions, and the chemical reaction mechanism of mixed fuels is key to understanding and guiding the control of in-cylinder ignition and combustion processes. In this work, a chemical reaction mechanism for the n-heptane/methane/ammonia blended fuel was developed using the Chemkin zero-dimensional homogeneous reactor model [32]. Several rate constants of elementary reactions were adjusted to improve accuracy, and the simplified mechanism was validated against the ignition delay times of pure methane, methane–ammonia blends, and n-heptane under high-pressure conditions. Using this mechanism, a chemical kinetics analysis under marine engine conditions was conducted.

2. n-Heptane/Methane/Ammonia Mechanism Construction and Validation

2.1. Construction of the n-Heptane/Methane/Ammonia Mixed Fuel Mechanism

Rahimi et al. [33] used CH_4 and n-C_7H_{16} as substitutes for natural gas and diesel, respectively, based on the GRI-Mech 3.0 and Valeri mechanisms. They employed a genetic algorithm to couple and simplify the chemical reactions, neglecting those with minimal impact on the combustion process, and adjusted the corresponding reaction rate constants to construct a simplified dual-fuel mechanism (containing 76 species and 464 elementary reactions). Subsequently, the simplified mechanism was coupled into the engine in-cylinder combustion simulation. Under different conditions, such as compression ratio, air-fuel ratio, and EGR (Exhaust Gas Recirculation) rate, the mechanism was validated with experimental results, which showed good agreement between the test and simulation. The 464-step Rahimi dual-fuel mechanism has been widely applied in three-dimensional engine simulations due to its good applicability in diesel-natural gas dual-fuel combus-

tion. The Otomo mechanism [14] performs well in predicting ammonia's ignition delay and laminar burning velocity. Therefore, this study uses both the Rahimi mechanism and the Otomo mechanism [14] to construct the multi-fuel reaction mechanism for n-heptane/methane/ammonia. After merging the two mechanisms, it is simplified based on different load thermal conditions of a medium-speed marine engine. In addition, some important cross-reactions between mixed fuels and intermediates are incorporated, and certain elementary reaction rate constants are adjusted based on experimental data. The simplified mechanism was then validated for ignition delay in different mixed fuels. In this study, DRGEP (Error Propagation Extension to Direct Relation Graph) and SA (Sensitivity Analysis) were adopted to reduce the detailed mechanism. The process of constructing the n-heptane/methane/ammonia mixed fuel chemical reaction mechanism is shown in Figure 1. The modifications to the rate constants of certain key elementary reactions are shown in Table 2. The mechanism includes the cross-reactions between methane/ammonia fuel intermediates, such as $CH_4 + NH_2 = CH_3 + NH_3$ and $CH_3 + NO_2 = CH_3O + NO$.

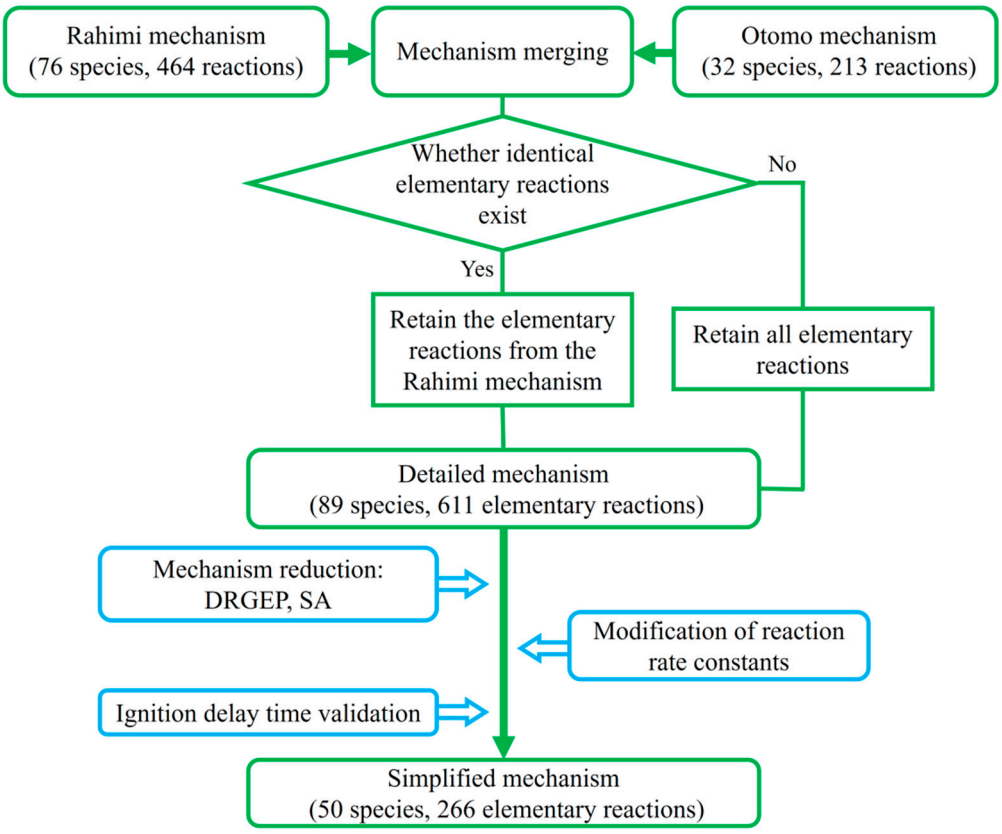


Figure 1. Flowchart for constructing $C_7H_{16}/CH_4/NH_3$ mixed fuel.

Table 2. Adjustment table for certain elementary reaction coefficients.

Serial Number	Elementary Reaction	A	n	E_a
R1	$NH_2 + HO_2 = NH_3 + O_2$	6.00×10^{18}	−1.9135	3.060×10^2
	DUP	5.90×10^7	1.5920	-1.373×10^3
R2	$NH_2 + HO_2 = H_2NO + OH$	1.00×10^{12}	0.1662	9.380×10^2
R3	$NH_2 + HO_2 = HNO + H_2O$	2.20×10^9	0.7906	-1.428×10^3
R4	$NH_2 + NO_2 = H_2NO + NO$	8.00×10^{11}	0.1100	-1.186×10^3
	DUP	-8.60×10^{17}	−1.8740	5.880×10^2
R5	$NH_2 + NO_2 = N_2O + H_2O$	8.60×10^{17}	−1.8740	5.880×10^2
R6	$CH_4 + NH_2 = CH_3 + NH_3$	7.50×10^3	3.0100	9.940×10^3
R7	$CH_3 + NO_2 = CH_3O + NO$	5.00×10^{13}	0.0000	0.0000

The adjustment of the elementary reaction rate constants in Table 2 refers to the following papers [34–36]. The n-heptane/methane/ammonia mixed fuel mechanism constructed in this study is mainly applied to the simulation optimization of diesel micro-ignition medium-speed marine engines, with methane as the primary fuel, a small amount of ammonia mixed in, and a trace amount of n-heptane to provide stable ignition energy. Therefore, in the process of mechanism merging, the Rahimi dual-fuel mechanism is used as the primary mechanism. This mechanism retains the complete GRI-Mech 3.0 mechanism. When conflicts arise between the Rahimi dual-fuel mechanism and the Otomo ammonia fuel mechanism, the elementary reactions from the Rahimi mechanism are retained.

2.2. Ignition Delay Validation of the n-Heptane/Methane/Ammonia Mechanism

In the simulation conditions of the marine engine, CH_4 is used as the primary fuel. Therefore, in the ignition delay time (IDT) verification section, the IDT of CH_4 under high-pressure conditions was first validated. The comparison between experimental data [37] and simulated methane IDT at different equivalence ratios under high-pressure conditions is shown in Figure 2a. The IDT predicted by the 266-step simplified mechanism is slightly higher than that predicted by the 611-step detailed mechanism, but both the 611-step detailed mechanism and the 266-step simplified mechanism provide good predictions of the methane IDT at different equivalence ratios when compared with the experimental results. Figure 2b compares the experimental data [38] and simulated methane IDT at pressures close to the engine compression and combustion pressures. The results show that the methane IDT predicted by the constructed mixed-fuel mechanism is in good agreement with the experimental results. This verifies that the n-heptane/methane/ammonia mixed fuel mechanism we developed can accurately predict the IDT of pure methane under high backpressure conditions.

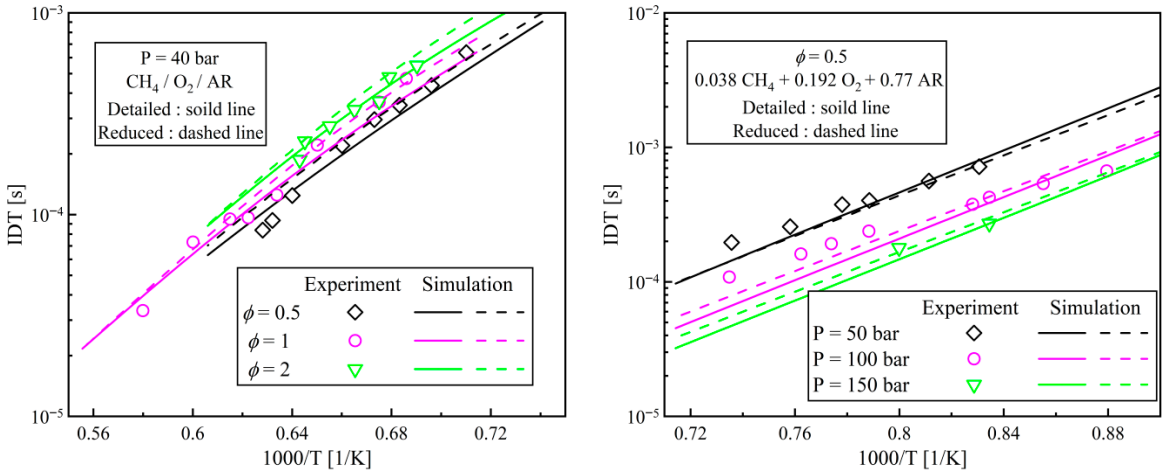


Figure 2. Comparison of experimental and calculated methane ignition delay under high-pressure conditions. (**a**) Different equivalence ratios; (**b**) Different pressure.

In recent years, countries around the world have increasingly focused on carbon emissions. Consequently, adopting appropriate technological measures to reduce carbon emissions is an important development direction for future marine engines. This paper first constructs an n-heptane/methane/ammonia mixed fuel chemical reaction mechanism. In the marine engine, CH_4 and NH3 are premixed and introduced into the cylinder to mix with air. Therefore, studying the ignition delay time (IDT) of CH_4 and NH_3 mixtures is crucial. Figure 3 presents a comparison of the experimentally measured and numerically predicted ignition delay times (IDTs) at various ammonia blending ratios under an equiv-

alence ratio of 0.5 and ambient pressures of 15 and 25 bar. The experimental data from Tsinghua University's RCM (Rapid Compression Machine) tests [36] are compared with the calculation results from the n-heptane/methane/ammonia mixed fuel chemical reaction mechanism constructed in this paper. The experimental and simulated results show good consistency, thereby validating that the constructed n-heptane/methane/ammonia mixed fuel mechanism can accurately predict the IDT in the CH_4 and NH_3 mixed atmosphere. The comparison of the IDT at high ammonia mixing ratios, as shown in Figure 4, reveals that the experimental and simulation results still show good consistency in high ammonia ratio atmospheres, further validating the rationality of the n-heptane/methane/ammonia mixed fuel reaction mechanism.

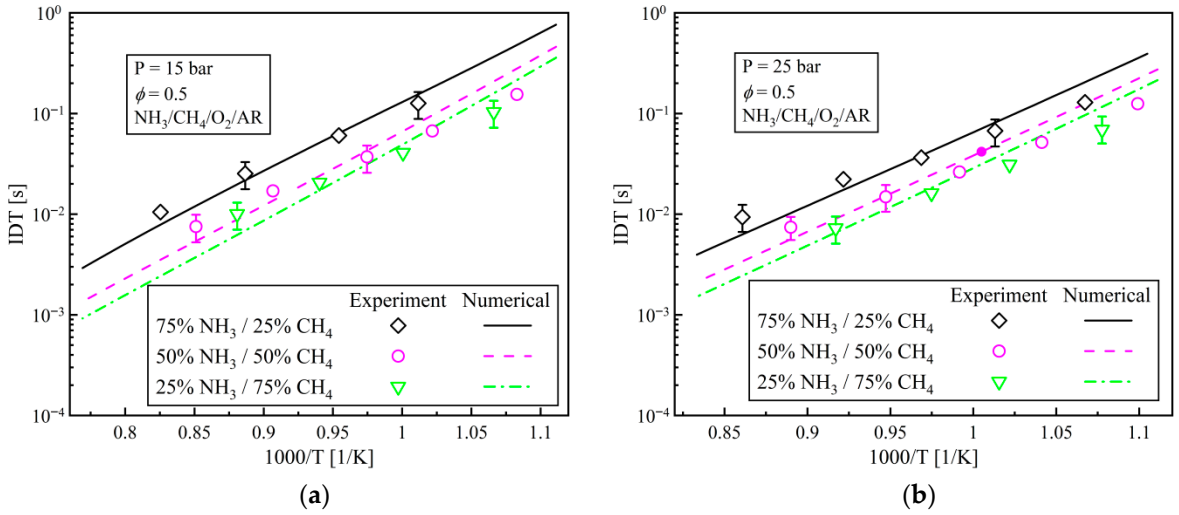


Figure 3. Comparison of experimental and calculated ignition delay for different ammonia blending ratios. (**a**) Pressure 15 bar; (**b**) Pressure 25 bar.

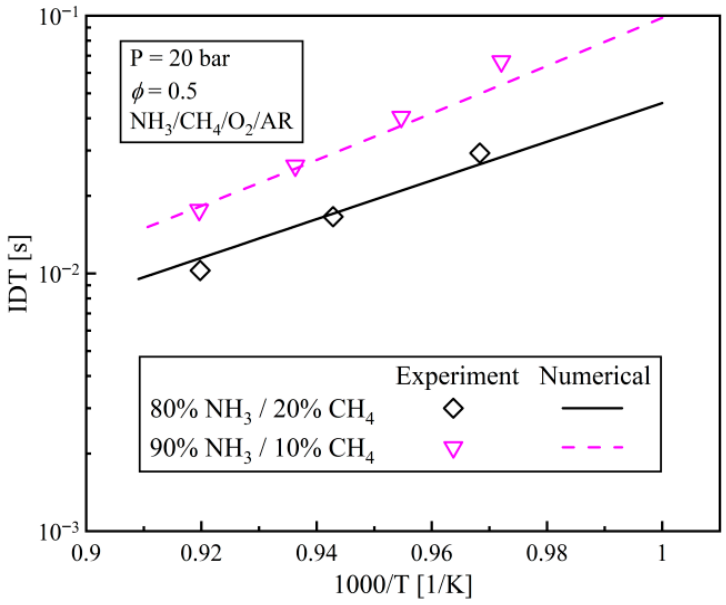


Figure 4. Comparison of experimental and calculated ignition delay at high ammonia blending ratios.

The comparison of the n-heptane IDT under different equivalence ratios is shown in Figure 5. The calculated n-heptane IDT using the n-heptane/methane/ammonia mixed fuel reaction mechanism developed in this study agrees well with the experimental measurement results [39] and can accurately predict the n-heptane NTC region. Additionally, it can be observed from the figure that the NTC region for n-heptane at a pressure of 41 bar

is narrower compared to the NTC region at 13.5 bar. This section separately validates the IDT of methane, methane mixed with ammonia, and n-heptane under high-pressure conditions, thus confirming the validity of the n-heptane/methane/ammonia mixed fuel reaction mechanism. In the future, this mechanism will continue to be used to further explore and reveal the IDT characteristics of the n-heptane/methane/ammonia mixed fuel.

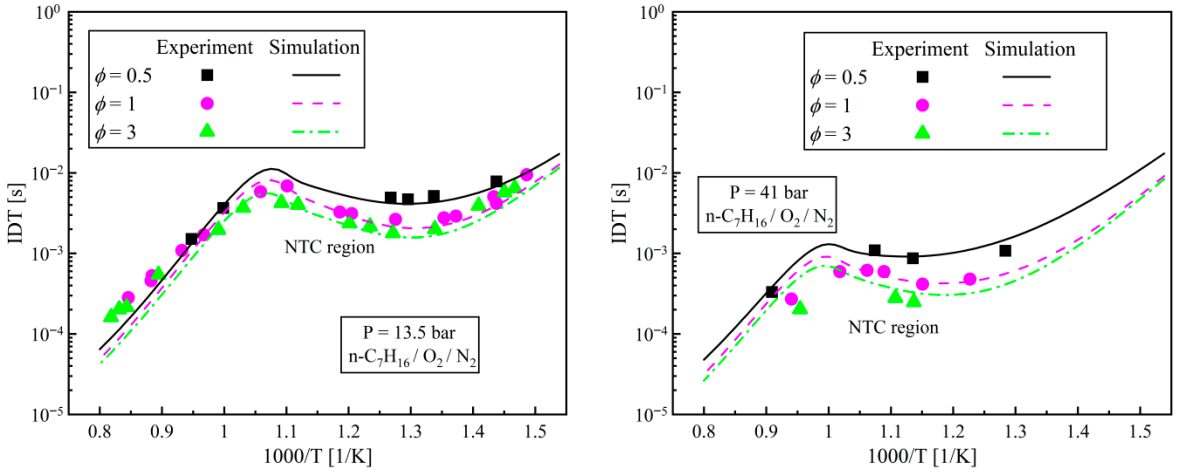


Figure 5. Comparison of ignition delay for n-heptane under different equivalence ratio conditions. (**a**) Pressure 13.5 bar; (**b**) Pressure 41 bar.

3. Results and Discussion

3.1. Effect of Environmental Parameters on the Ignition Process of n-Heptane/Methane/Ammonia Mixed Fuel

3.1.1. Effect of a Single Parameter on Ignition Delay

The n-heptane/methane/ammonia chemical reaction mechanism was developed specifically for marine engine operating conditions, where n-heptane is used as the ignition fuel, and methane and ammonia are premixed through port injection prior to combustion. Therefore, the IDT characteristics discussed in this section are focused on the temperature range of 800–1200 K, pressure range of 40–180 bar, and equivalence ratio range of 0.5–3. Considering that the n-heptane/methane/ammonia mixing ratio changes cooperatively, during the diesel spray process in the engine, the diesel fuel undergoes atomization, evaporation, and continuous absorption of the surrounding mixed gas. Thus, the molar fraction of n-C_7H_{16} in the fuel is set to vary between 10–60%. To control the variables, the molar fraction ratio of CH_4 and NH_3 is fixed at 1. When discussing the effect of NH_3 molar fraction on IDT, the molar fraction of n-C_7H_{16} is fixed at 10%, and the molar fraction of CH_4 changes with the molar fraction of NH_3. Considering the relatively low reactivity of ammonia, methane remains the primary fuel under practical operating conditions, while ammonia serves as an auxiliary fuel. Therefore, the ammonia molar fraction is limited to within 50%. The influence of the molar fraction of ammonia fuel on IDT is the key focus of this section. The range of initial parameters is shown in Table 3.

Table 3. Initial parameters setting range.

Parameters	Range	Controlled Variable
Temperature (K)	800–1200	1000
Pressure (MPa)	4–18	5
Equivalence ratio	0.5–3	1
$Y_{n\text{-}C7H16}$	10–60%	10%
Y_{CH4}	40–90%	-
Y_{NH3}	0–50%	-
Y_{CH4}/Y_{NH3}	-	1

First, the effect of individual factors on the ignition delay time (IDT) of n-heptane/methane/ammonia mixed fuel was studied using the method of controlling variables. The IDT of the mixed fuel with a molar fraction of n-C_7H_{16} of 10% and a molar ratio of CH_4 to NH_3 of 1, as a function of temperature, is shown in Figure 6. N-C_7H_{16} exhibits a two-stage ignition process. During the pyrolysis of n-C_7H_{16}, some low-activity intermediate products are formed, which are not easily reactive at medium to low temperatures. This results in the ignition delay time of n-C_7H_{16} increasing with temperature, a phenomenon known as the negative temperature coefficient (NTC) phenomenon. As shown in Figure 6a, the effect of environmental pressure on the ignition delay time of the mixed fuel is very regular under the same initial equivalence ratio. As the pressure increases, the ignition delay time decreases gradually, and the overall negative temperature coefficient phenomenon becomes less pronounced. On one hand, CH_4 and NH_3 do not exhibit the negative temperature coefficient phenomenon during combustion. The reactivity of CH_4 and NH_3 is lower than that of the intermediate products formed during the medium-temperature ignition stage of n-C_7H_{16}. With a combined molar fraction of CH_4 and NH_3 at 90%, this significantly weakens the NTC phenomenon of n-C_7H_{16}. On the other hand, high-pressure thermal conditions increase the reactivity of the intermediate products generated during the pyrolysis of n-C_7H_{16}. The probability of collisions between these free intermediate products increases under high pressure, which in turn increases the probability of bond cleavage and reorganization. This is the fundamental reason for the increased reactivity, which also somewhat weakens the negative temperature coefficient phenomenon. The effect of initial equivalence ratio on the ignition delay time is shown in Figure 6b. As the equivalence ratio increases, the ignition delay time decreases gradually. When the initial equivalence ratios are 2, 2.5, and 3, the changes in ignition delay time are relatively small. When the initial equivalence ratio is 0.5, its ignition delay time differs significantly from other equivalence ratios, and the negative temperature coefficient phenomenon is least pronounced at this equivalence ratio. Under the same initial pressure, the continuous decrease in equivalence ratio reduces the molar ratio of fuel to air in the mixture. This can be understood as a gradual decrease in fuel amount and an increase in air volume in a confined space. This leads to a reduction in the low-activity intermediate products formed during the pyrolysis of n-C_7H_{16}, thereby weakening the negative temperature coefficient phenomenon in the mixed fuel.

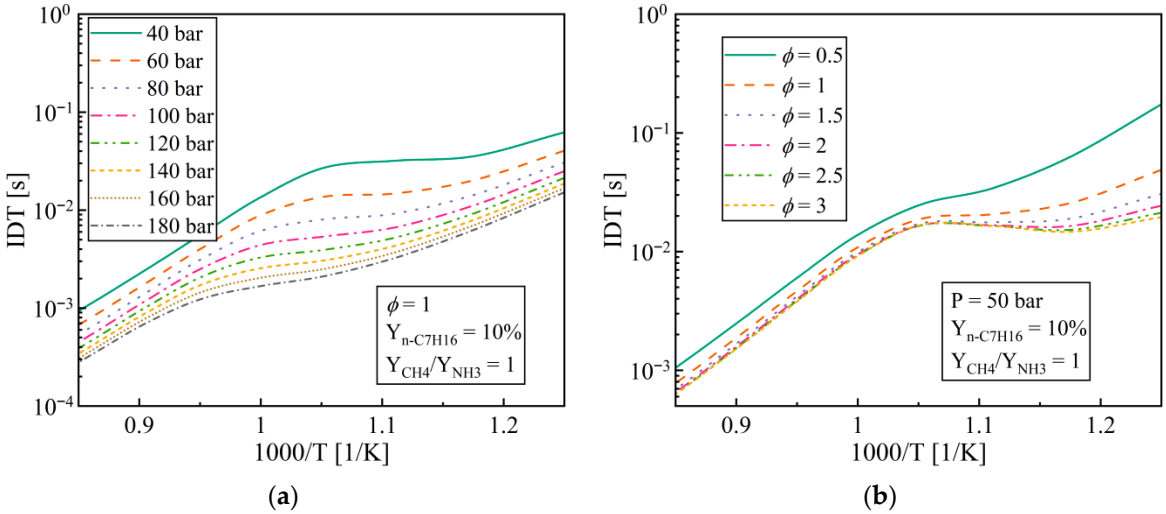


Figure 6. Variation of ignition delay with temperature for mixed fuel with 10% molar fraction of n-C7H16 and a CH_4 to NH_3 molar ratio of 1. (**a**) Effect of different pressures; (**b**) Effect of different equivalence ratios.

The variation of ignition delay time (IDT) of n-heptane/methane/ammonia mixed fuel with temperature under an initial pressure of 50 bar and equivalence ratio of 1 is shown in Figure 7. Figure 7a shows the effect of different n-C_7H_{16} molar fractions on the ignition delay time of the mixed fuel. As the n-C_7H_{16} molar fraction increases, the ignition delay time gradually decreases. When the n-C_7H_{16} molar fractions are 40%, 50%, and 60%, the change in ignition delay time becomes smaller. It can be observed that under an initial pressure of 50 bar and an equivalence ratio of 1, increasing the n-C_7H_{16} molar fraction to 40% results in a very weak effect on the ignition delay time when further increases are made to the n-C_7H_{16} molar fraction. The effect of different NH_3 molar fractions on the ignition delay time is shown in Figure 7b. From the figure, it can be seen that the ignition delay time shows an opposite trend in different temperature ranges. When the temperature range is 800 K to 900 K, the ignition delay time of the mixed fuel decreases with increasing NH_3 molar fraction. However, when the temperature range is 900 K to 1200 K, the ignition delay time of the mixed fuel increases with increasing NH_3 molar fraction. It can thus be concluded that as the NH_3 molar fraction increases, the negative temperature coefficient phenomenon exhibited by the n-heptane/methane/ammonia mixed fuel ignition delay time becomes more pronounced. The theoretical air-fuel ratios of CH_4 and NH_3 are 17.2 and 6.1, respectively. As the NH_3 molar fraction increases and the CH_4 molar fraction decreases, the amount of air in the confined space decreases, i.e., the number of N_2 and O_2 molecules decreases, while the number of n-C_7H_{16} molecules in the space remains unchanged. Therefore, under the same pressure and equivalence ratio, the number of low-activity intermediate products generated from the pyrolysis of n-C_7H_{16} remains unchanged. However, the collision probability between these free low-activity intermediate products and oxygen atoms in the confined space greatly decreases, resulting in lower conversion efficiency. The low-activity intermediate products generated by the pyrolysis of n-C_7H_{16} are dependent on oxygen atoms. When the O_2 concentration decreases, these intermediate products gradually accumulate in the medium-to-low temperature environment, thereby intensifying the negative temperature coefficient phenomenon.

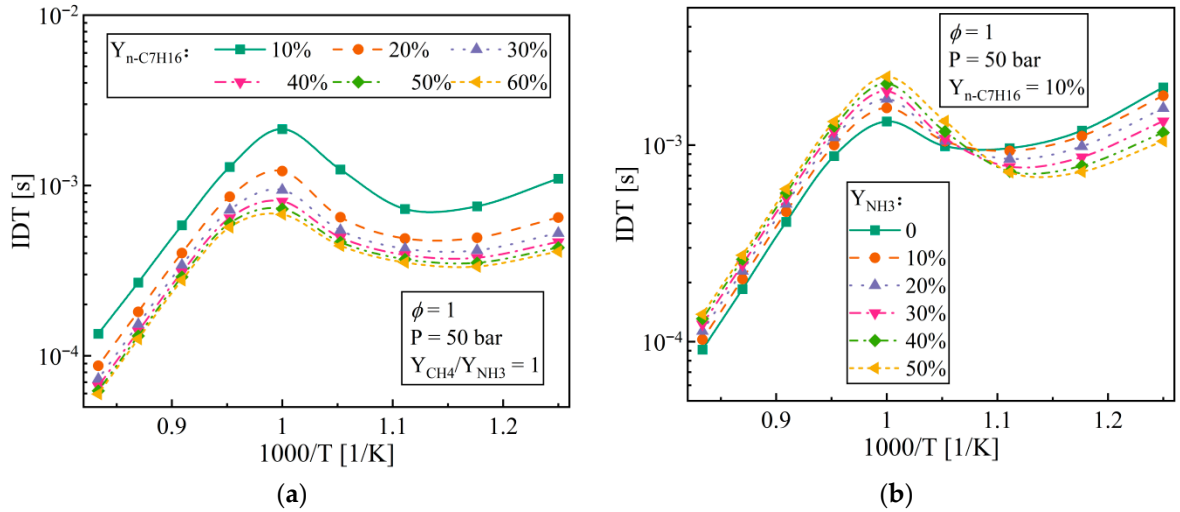


Figure 7. Variation of ignition delay with temperature for mixed fuel at an initial pressure of 50 bar and an equivalence ratio of 1. (**a**) Effect of varying n-C7H16 molar fractions; (**b**) Effect of varying NH3 molar fractions.

3.1.2. Effect of Multiple Parameters on Ignition Delay

The effects of different pressure, temperature, equivalence ratio, n-C_7H_{16} molar fraction, and NH_3 molar fraction on the ignition delay time (IDT) of n-heptane/methane/ammonia mixed fuel are shown in Figure 8. The effect of different pressures and initial temperatures on the IDT is shown in Figure 8a. At the same initial temperature, as the pressure increases, the IDT shows a gradually decreasing trend. The high-IDT region appears at low pressures and initial temperatures of 800 K and 1000 K. From the pressure and temperature contour plots, it can also be observed that the mixed fuel exhibits a clear negative temperature coefficient (NTC) phenomenon, which progressively shifts toward higher temperature regions with increasing pressure. The effect of different equivalence ratios and initial temperatures on the IDT is shown in Figure 8b. The high-IDT region appears at low equivalence ratios and temperatures of 800 K and 1000 K. At a temperature of 800 K, there is no significant change in the IDT when the equivalence ratio varies between 1.5 and 3. At temperatures exceeding 1100 K, the IDT is less affected by the equivalence ratio.

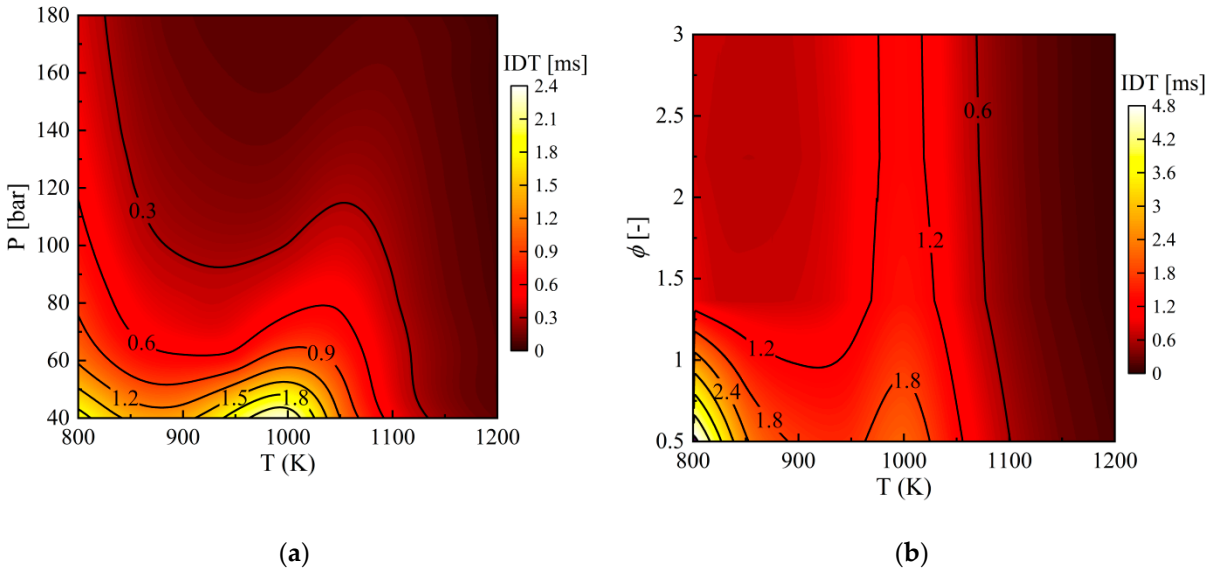


Figure 8. Effects of different pressures, temperatures, and equivalence ratios on the ignition delay of mixed fuel. (**a**) Effect of different pressures; (**b**) Effect of different equivalence ratios.

The effect of different n-C_7H_{16} molar fractions on the IDT is shown in Figure 9a. When the temperature is above 1100 K, the IDT is less affected by the n-C_7H_{16} molar fraction. When the temperature range is between 900 K and 1000 K, the IDT shows a gradual extension with increasing temperature and decreasing n-C_7H_{16} molar fraction. When the temperature range is between 1000 K and 1100 K, the IDT shows a gradual decrease with increasing temperature and n-C_7H_{16} molar fraction. A very clear negative temperature coefficient (NTC) phenomenon can also be observed in Figure 9a, with the inflection point of the NTC always occurring at temperatures between 900 K and 1000 K. This indicates that the initial pressure and equivalence ratio have a greater influence on the NTC phenomenon, while the n-C_7H_{16} molar fraction has a smaller effect, which is consistent with the findings in Figure 7a. The effect of NH_3 molar fraction on the IDT at different initial temperatures is shown in Figure 9b. When the temperature range is between 800 K and 900 K, a longer IDT appears in the low temperature and low NH_3 molar fraction region. As mentioned earlier, the decrease in NH_3 molar fraction at the same equivalence ratio leads to a decrease in O2 concentration, and low temperatures also suppress the reactivity of the mixed fuel, ultimately resulting in a longer IDT. When the temperature range is between 900 K and 1000 K, a longer IDT appears in the high temperature and high NH_3 molar fraction region. The main reason for this trend is the significantly enhanced cracking of n-C_7H_{16} in this temperature range. At 1000 K with an NH_3 molar fraction of 0.5, n-C_7H_{16} produces a large number of low-activity intermediate products under the influence of temperature and high O_2 concentration, further delaying the IDT of the mixed fuel due to these intermediate products' action. When the temperature exceeds 1000 K, a longer IDT appears in the low temperature and high NH3 molar fraction region. In this region, the IDT is still affected by the low-activity intermediate products produced by n-C_7H_{16} cracking. As the temperature increases, the effect of NH_3 molar fraction on the IDT becomes smaller. After the temperature exceeds 1100 K, the effects of pressure, equivalence ratio, n-C_7H_{16}, and NH_3 molar fraction on the IDT significantly decrease.

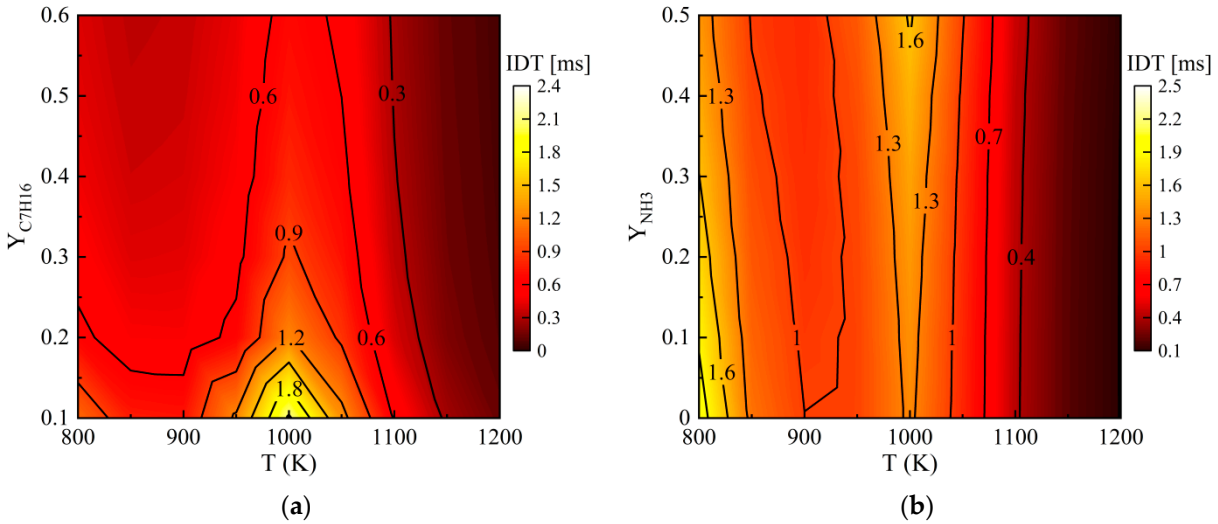


Figure 9. Effects of different temperatures, n-C7H16 molar fractions, and NH_3 molar fractions on the ignition delay of mixed fuel. (**a**) Effect of varying n-C7H16 molar fractions; (**b**) Effect of varying NH3 molar fractions.

The effects of different pressures, equivalence ratios, and NH_3 molar fractions on the ignition delay time (IDT) of n-C_7H_{16}/CH_4/NH_3 mixed fuel at an initial temperature of 1000 K are shown in Figure 10. The influence of different pressures and equivalence ratios on the IDT is shown in Figure 10a. At the same equivalence ratio, the IDT gradually

decreases as the initial pressure increases, and when the initial pressure is between 120 and 180 bar, the range of change in IDT is smaller. At the same initial pressure, the IDT is less affected by changes in equivalence ratio. The effect of different NH3 molar fractions and equivalence ratios on the IDT is shown in Figure 10b. At the same NH_3 molar fraction, the IDT is less affected by changes in equivalence ratio. When the equivalence ratio is below 1.5, the IDT is influenced by both the NH_3 molar fraction and the equivalence ratio. In this case, longer ignition delays are observed in regions with higher NH_3 molar fractions and lower equivalence ratios, as increasing NH_3 molar fraction and decreasing equivalence ratio slow down the fuel decomposition rate, thereby extending the IDT. When the equivalence ratio exceeds 1.5, the IDT gradually increases with the increase of NH_3 molar fraction. This indicates that the addition of ammonia inhibits the ignition process of the mixed fuel. The influence of ammonia will be further explored in subsequent analyses. The effect of different NH_3 molar fractions and initial pressures on the IDT is shown in Figure 10c. At the same initial pressure, the IDT is less affected by changes in NH_3 molar fraction. As the initial pressure increases, the IDT gradually decreases. In the high-pressure region, when the initial pressure exceeds 100 bar, the change gradient of the IDT becomes smaller. However, when the initial pressure is between 40 and 80 bar, there is a larger change gradient in the IDT, which is consistent with the influence of initial pressure on the IDT shown in Figure 10a. The influence of initial pressure on the IDT is most significant when the initial pressure varies between 40 bar and 80 bar, and the IDT is more influenced by the NH3 molar fraction than by the equivalence ratio. This provides theoretical support for the optimization process of mixed fuel application in medium-speed marine engines.

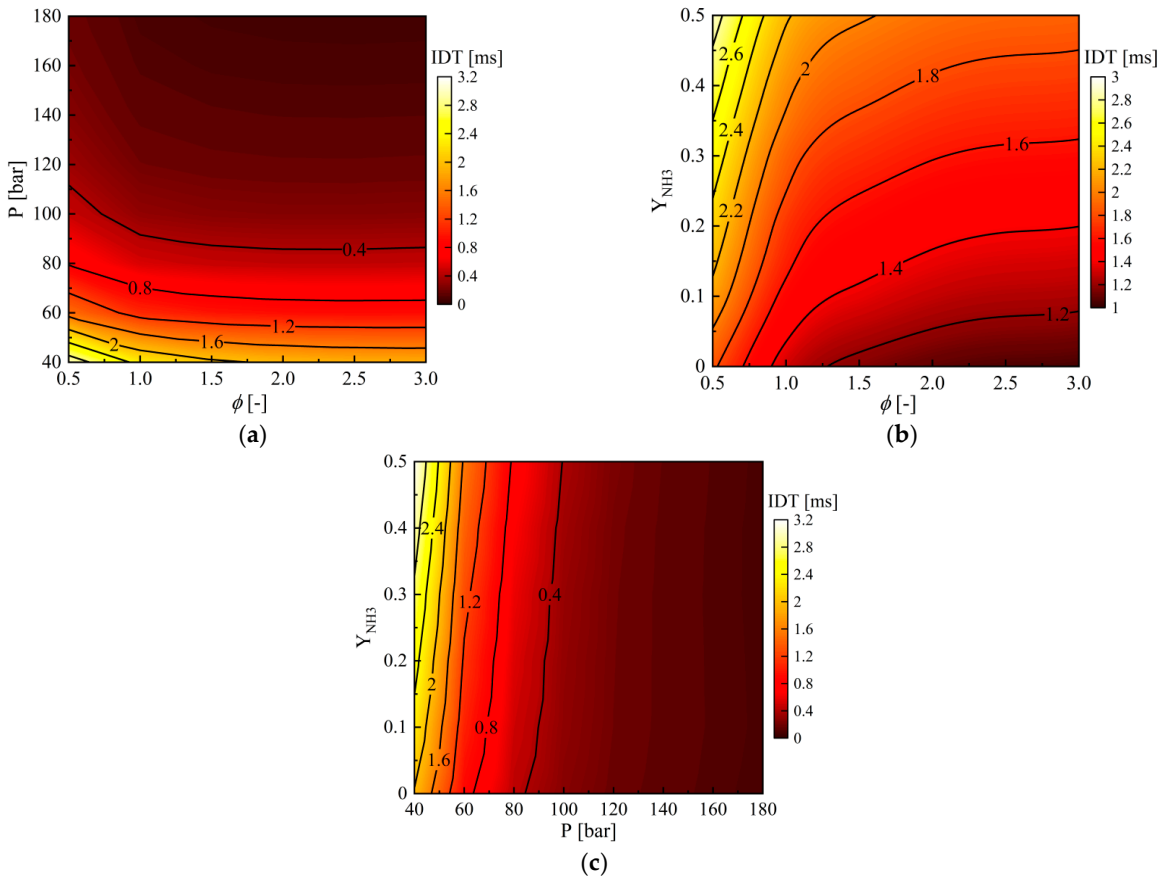


Figure 10. Effects of different pressures, equivalence ratios, and NH_3 molar fractions on the ignition delay of mixed fuel at an initial temperature of 1000 K. (**a**) Effect of varying pressure and equivalence ratio; (**b**) Effect of varying NH_3 mole fraction and equivalence ratio; (**c**) Effect of varying NH_3 mole fraction and initial pressure.

3.2. Sensitivity Analysis of the Ignition Process for n-Heptane/Methane/Ammonia Mixed Fuel

To comprehensively analyze the effects of various variables on combustion characteristics, a sensitivity analysis method was used. This method is used to identify key components and free radicals in the local flame zone that significantly contribute to combustion, which directly or indirectly participate in reactions. The normalized matrix of the local sensitivity coefficients (S^n) can be expressed as:

$$S^n = \left(\frac{k_{fi}}{X_j} \frac{\partial X_j}{\partial k_{fi}} \right) = \left(\frac{\partial ln X_j}{\partial ln k_{fi}} \right) \quad (1)$$

In the Equation (1), $\frac{X_j}{\partial k_{fi}}$ represents the sensitivity coefficient of the concentration of the *j*-th component relative to the rate constant of the *i*-th reaction.

The ignition process of the mixed fuel is measured by temperature, with the ignition delay defined as the period when the temperature exceeds 1800 K. Temperature variations directly reflect the ignition process. Therefore, the top 12 reactions with the greatest impact on temperature were selected, and the sensitivity coefficients of each elementary reaction were normalized. A positive sensitivity coefficient indicates that the elementary reaction promotes the ignition process, while a negative value indicates that it suppresses the ignition process. The larger the absolute value, the greater the impact on the ignition process.

The sensitivity analysis of the n-C_7H_{16} molar fraction on the ignition delay of the mixed fuel at an initial temperature of 800 K is shown in Figure 11. When the n-C_7H_{16} molar fraction is 0.1, the four reactions R67, R135, R60, and R255 dominate the ignition process. Among them, R67 and R135 promote the ignition process. As the n-C_7H_{16} molar fraction increases, the promoting effect of R67 and R135 gradually weakens. R146 and R49 are less affected by the n-C_7H_{16} molar fraction and gradually become the reactions with the greatest influence on the ignition process. R146 is an important branching reaction. This reaction pathway directly promotes the formation of hydrogen peroxide ketone, which, as a branching agent, generates new radicals. It promotes the accumulation of CH_2O and H_2O_2 in the radical pool, which are two characteristic substances of low-temperature reactions in the n-heptane combustion process. The sensitivity analysis diagram also shows that R60 and R255 inhibit the ignition process. After NH_3 is mixed into the fuel, its reaction with O2 causes a competitive relationship between NH_3 and other fuels. As the n-C_7H_{16} molar fraction in the fuel increases, the proportion of NH_3 decreases, and the inhibitory effect of the R255 reaction on the ignition process significantly decreases.

The sensitivity analysis of the n-C_7H_{16} molar fraction on the ignition delay of the mixed fuel at an initial temperature of 1000 K is shown in Figure 12. The R146 reaction plays a dominant role in promoting ignition, while the promoting effect of R67 and R135 on the ignition process is lower than that of R146. As the n-C_7H_{16} molar fraction increases, the influence of R146, R67, and R135 shows a gradually decreasing trend. The increase in the n-C_7H_{16} molar fraction simultaneously drives the decrease in the NH_3 molar fraction, leading to a decrease in O2 concentration. This directly affects the OH concentration in the radical pool, which partially inhibits the cracking of n-C_7H_{16}. The R152: C7H15-2 = CH3 + C6H12O reaction plays a dominant role in inhibiting the ignition process, and this inhibitory effect outweighs the promoting effect of R146.

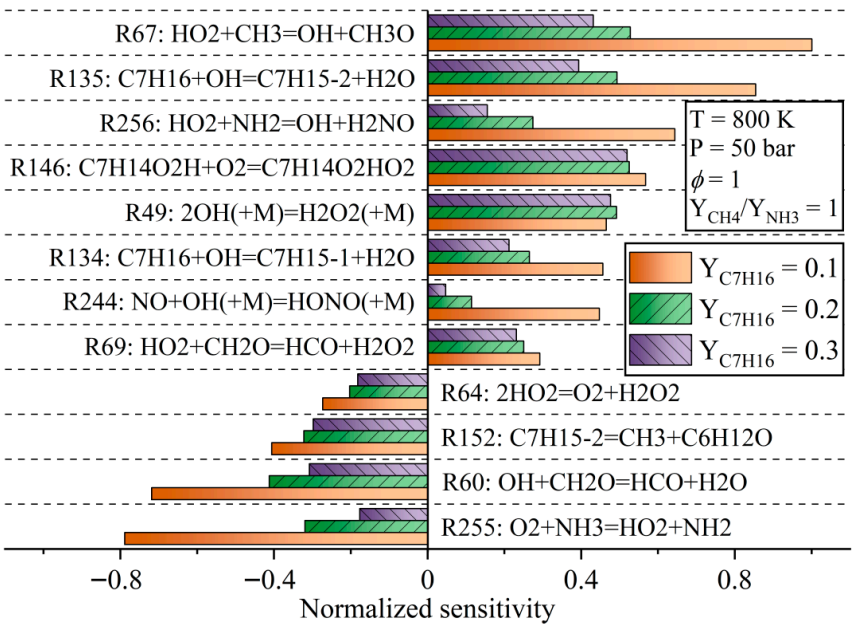


Figure 11. Sensitivity analysis of n-C_7H_{16} molar fraction on ignition delay of mixed fuel at an initial temperature of 800 K.

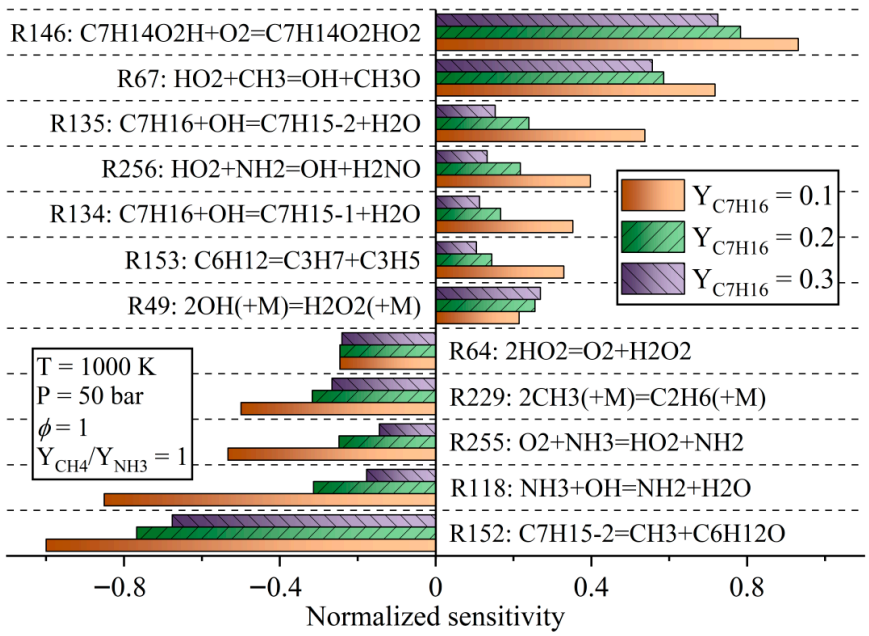


Figure 12. Sensitivity analysis of n-C_7H_{16} molar fraction on ignition delay of mixed fuel at an initial temperature of 1000 K.

The sensitivity analysis of the NH_3 molar fraction on the ignition delay of the mixed fuel at an initial temperature of 800 K is shown in Figure 13. The R49, R135, and R67 reactions have a dominant promoting effect on the ignition process. As the NH_3 molar fraction increases, this promoting effect gradually weakens, indicating that the increase in NH_3 concentration has an inhibitory effect on the ignition process, which is consistent with the results analyzed in Figure 10b. In the reaction system, after the incorporation of ammonia fuel, it competes with other fuels for oxygen resources, leading to a slowdown in the oxidation processes of other fuels and radicals, for example, R146, where the increase in ammonia concentration partially inhibits the formation of hydrogen peroxide ketone, As mentioned earlier, hydrogen peroxide ketone plays a combustion-promoting role during

the ignition process. As the NH_3 concentration increases, the sensitivity of R255 becomes progressively higher, which further indicates that the increase in NH_3 concentration has an inhibitory effect on the ignition process.

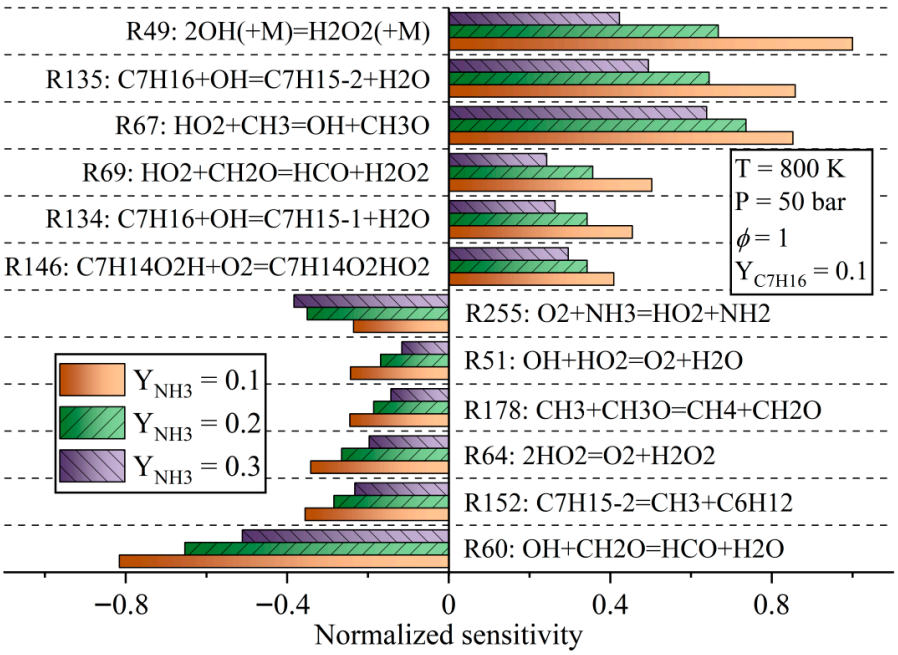


Figure 13. Sensitivity analysis of NH_3 molar fraction on ignition delay of mixed fuel at an initial temperature of 800 K.

The sensitivity analysis of NH_3 molar fraction on the ignition delay time of the mixed fuel at an initial temperature of 1000 K is shown in Figure 14. Unlike the environment at an initial temperature of 800 K, R67 and R146 become the most sensitive reactions promoting ignition. As the NH_3 molar fraction increases, the sensitivity of R67 gradually decreases. The concentration of CH_4 in the fuel directly affects the formation process of CH_3, and as the NH_3 molar fraction increases, the CH_4 molar fraction decreases, thus limiting the forward reaction of R67. While the sensitivity of R146 does not decrease with the increase of NH_3 molar fraction, it slightly increases, indicating that at an initial temperature of 1000 K, the formation process of hydrogen peroxide ketone is less affected by NH_3 molar fraction, with temperature being the key factor influencing its formation. From the variation of R118 sensitivity, it can be observed that the reaction between NH_3 and OH shows higher sensitivity at an initial temperature of 1000 K. As the NH_3 molar fraction increases, R118 increasingly inhibits the ignition process. At an initial temperature of 1000 K, R152 has the strongest inhibitory effect on the ignition process. C7H15-2, one of the main low-activity intermediates during n-C_7H_{16} pyrolysis, is less affected by the NH3 molar fraction at 1000 K, leading to the formation of a large amount of low-activity intermediates, which suppress the further temperature rise. This is the main reason for the negative temperature coefficient (NTC) phenomenon. The pyrolysis reactions of n-C_7H_{16}, R134 and R135, show opposite trends with changes in NH_3 molar fraction at initial temperatures of 800 K and 1000 K, indicating that the initial temperature is a key factor affecting the pyrolysis process of n-C_7H_{16}. At an initial temperature of 1000 K, as the NH_3 molar fraction increases, the sensitivity coefficient of R134 and R135 gradually increases, suggesting that the increased NH_3 concentration accelerates the pyrolysis rate of n-C_7H_{16}.

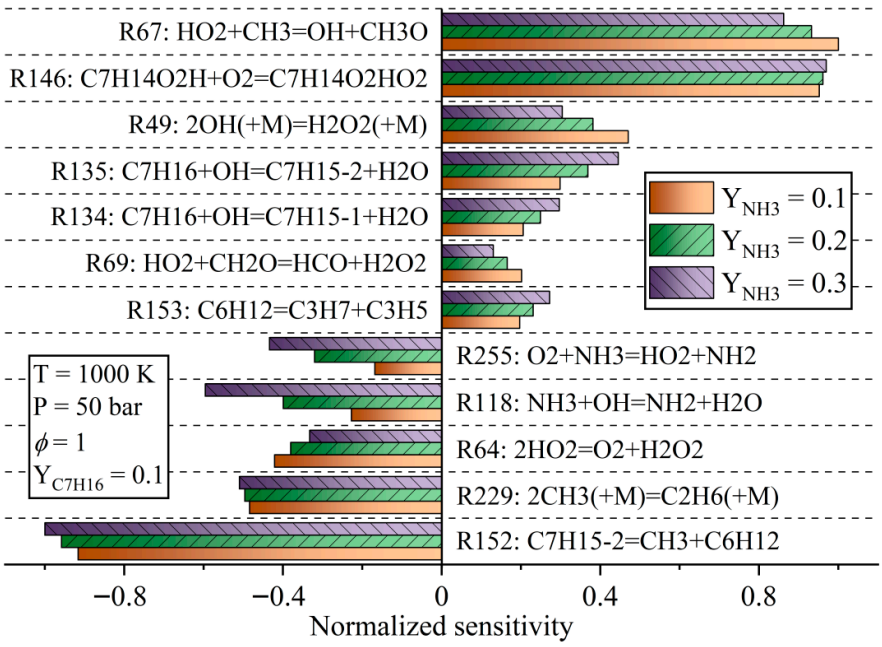


Figure 14. Sensitivity analysis of NH_3 molar fraction on ignition delay of mixed fuel at an initial temperature of 1000 K.

3.3. Chemical Kinetic Analysis of the Ignition Process for n-Heptane/Methane/Ammonia Mixed Fuel

To further understand the ignition process of n-heptane/methane/ammonia mixed fuels, the time-dependent variations of fuel and certain radical mole fractions before ignition were analyzed. The variations in mole fractions of the radicals CH_2O, H_2O_2, OH and temperature over time are shown in Figure 15. During the low-temperature reaction stage, CH_2O and H_2O_2 accumulate significantly in the radical pool. As time progresses, the mole fraction of CH_2O remains relatively low, while H_2O_2 exhibits a slow increasing trend. At the same time, the mole fraction of n-C_7H_{16} shows a slow decline, and the mole fractions of CH_4 and NH_3 remain almost unchanged. This indicates that the accumulation of CH_2O and H_2O_2 in the radical pool is primarily attributed to the n-C_7H_{16} cracking process. As the ammonia energy fraction increases, the ignition delay time shows a delayed trend. An increase in ammonia energy fraction leads to a decrease in oxygen concentration, which further delays the high-temperature reactions of diesel.

In Figure 15, it can be observed that at lower concentrations of NH_3, the n-C_7H_{16} cracking rate is faster. As the temperature increases, the CH_2O and H_2O_2 radicals are rapidly consumed. After a brief delay, OH radicals quickly accumulate, and the temperature increases sharply. Under the initial conditions of 800 K, 50 bar pressure, and an equivalence ratio of 1, the ignition delay is shorter for cases with higher NH_3 concentrations. The rate of n-C_7H_{16} consumption at different times is analyzed in Figure 16, which lists the two most important cracking reactions, R138 and R139, in the consumption of n-C_7H_{16}. n-C_7H_{16} exhibits a multi-stage ignition process at low temperatures. Under the initial conditions of 800 K, the first stage of n-C_7H_{16} consumption occurs between 0.15 to 0.25 ms, with more than 60% of the total n-C_7H_{16} consumed rapidly in this stage. At this point, as the NH_3 molar fraction increases, the key cracking reactions, R138 and R139, are delayed. From Figure 16b, it can be seen that the second stage of n-C_7H_{16} consumption occurs between 0.5 to 1.8 ms. During this phase, the consumption rate of n-C_7H_{16} slows down, and with the increase in NH_3 molar fraction, reactions R138 and R139 occur earlier. At 800 K, the first stage of rapid n-C_7H_{16} cracking causes a slight increase in temperature, while the second stage of slower cracking occurs at 1000 K. Combining the sensitivity

analysis in Figure 15, it can be observed that the sensitivity of the key cracking reactions, R138 and R139, increases significantly with the increase in NH_3 molar fraction. At 1000 K, the increase in NH_3 molar fraction leads to a decrease in CH_4 concentration, which weakens the inhibitive effect of CH_4 on n-C_7H_{16} cracking. The higher the NH_3 concentration, the more intense the competition for OH radicals. After NH_3 undergoes initial decomposition, the produced NH_2 has a weaker competition for OH radicals than n-C_7H_{16}, thus enhancing OH participation in n-C_7H_{16} cracking reactions.

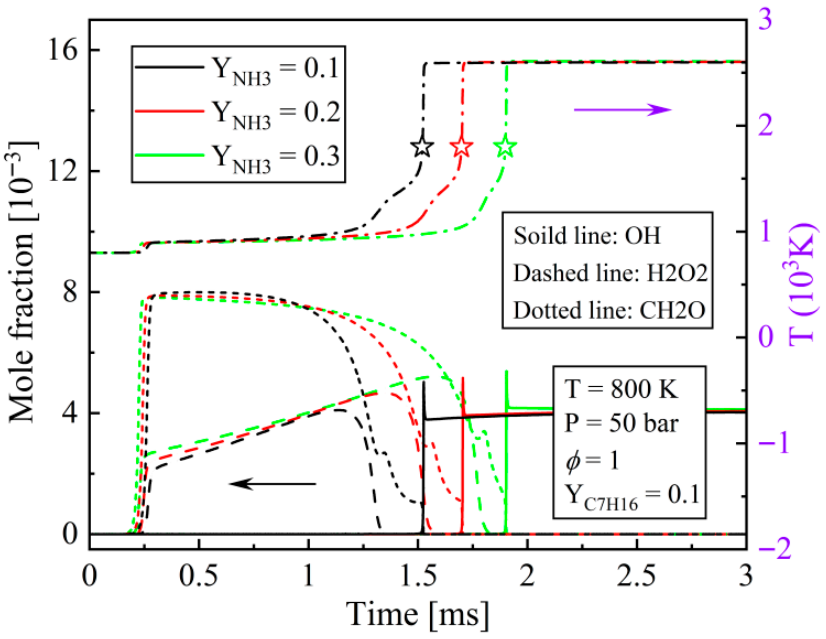


Figure 15. Variation of representative radical molar fractions and temperature at different NH_3 molar fractions (pentagon markers indicate ignition time).

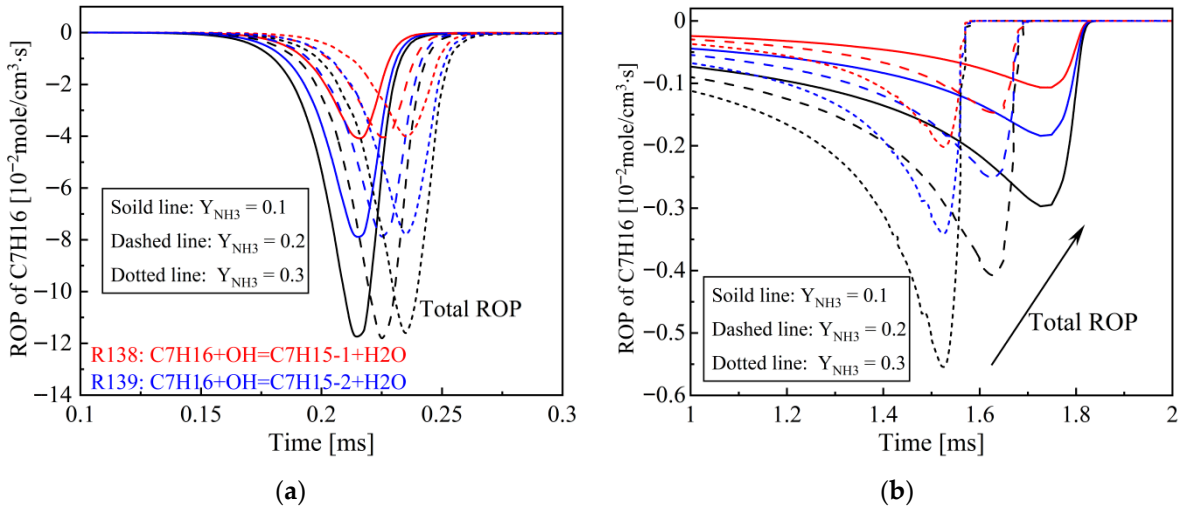


Figure 16. ROP analysis of n-C_7H_{16} at different NH_3 molar fractions. (**a**) Stage 1; (**b**) Stage 2.

The ROP analysis of CH_4, NH_3, CH_2O, and OH radicals at different NH_3 molar fractions is shown in Figure 17. It can be observed that the main consumption reactions of CH_4 and NH_3 are dehydrogenation reactions induced by O, H, and OH radicals. The production and consumption rates of the representative low-temperature radical CH_2O and the high-temperature representative radical OH are shown in Figure 17c,d. From the figure, it can be seen that the production and consumption of CH_2O occur earlier than that of OH radicals, with a brief transition period between the low-temperature and high-temperature

reactions. In the high-temperature stage, the methyl radical participates in reaction R7 (R7: O + CH3 = H + CH2O), which is the main production reaction of CH_2O. Most of the methyl radicals come from the dehydrogenation reaction of CH_4. In the low-temperature stage, reaction R191 (R191: C2H4 + OH = CH2O + CH3) is the main production reaction for H_2O, and all C_2H_4 comes from the cracking process of n-heptane (C7H16 → C7H15-2 → C7H15O2 → C7H14O2H → C7H14O2HO2 → C7KET21 → C2H4). Furthermore, in the low-temperature stage, reaction R191 is almost unaffected by the NH_3 molar fraction.

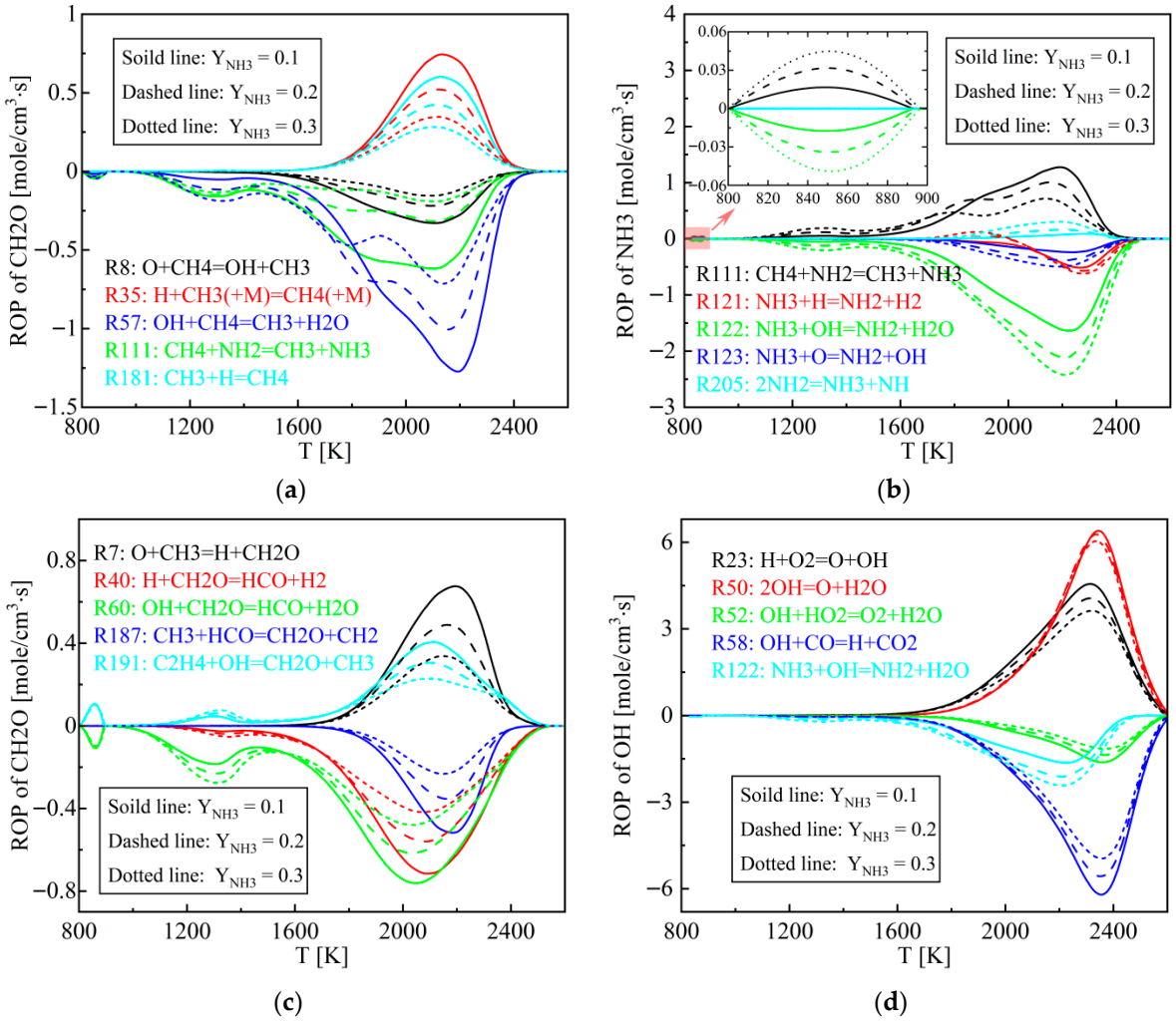


Figure 17. ROP analysis of CH_4, NH_3, CH_2O, and OH radicals at different NH_3 molar fractions. (**a**) CH_4; (**b**) NH_3; (**c**) CH_2O; (**d**) OH.

In marine engine emission regulations, there are strict standards for NO_x emissions, while in recent years, increasing attention has been focused on reducing carbon emissions from ship engines. N_2O and CO_2 are both important greenhouse gases that contribute to global warming. Although the use of ammonia-fueled combustion reduces carbon emissions, the presence of N_2O in the exhaust gas actually exacerbates the greenhouse effect. This is an important factor to consider when applying ammonia fuel in ship engines. Among all the intermediate products of ammonia combustion, N_2O, although present in low concentrations, is a potent greenhouse gas. Research has shown that N_2O has a global warming potential (GWP) 298 times greater than that of CO_2 [40]. The ROP analysis of NO and N_2O at different NH_3 molar fractions is shown in Figure 18. The generation of NO mainly depends on the reactions of N with O, O_2, and OH radicals. Among these, the reaction of N with O_2, R88 (R88: N + O2 → NO + O), has the greatest impact on NO's ROP, and

as the NH_3 molar fraction increases, the rate of NO generation by R88 reaction increases. This indicates that high-temperature oxygen-rich environments and higher ammonia blending ratios are more likely to produce NO emissions. N_2O generation mainly depends on the reaction of NH and NO in R105, and as the NH_3 molar fraction increases, the rate of N_2O generation by R105 reaction increases. N_2O consumption is mainly through reactions R92 and R94. The consumption process is more delayed than the generation process in R105, indicating that the N_2O consumption process is more temperature-dependent. The above results, based on a zero-dimensional homogeneous reactor, provide a theoretical basis for subsequent three-dimensional simulations of ammonia combustion in engines. Moreover, future research on medium-speed marine engines should take into account N_2O emissions.

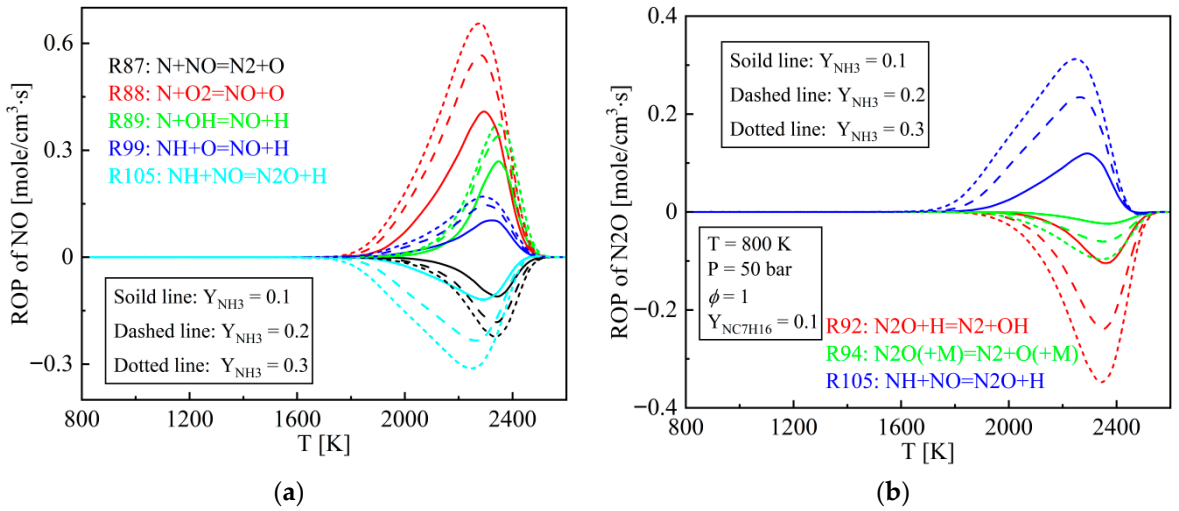


Figure 18. ROP analysis of NO and N_2O at different NH_3 molar fractions. (**a**) NO; (**b**) N_2O.

The presence of n-heptane in the mixed fuel causes the overall combustion process to exhibit multi-stage ignition characteristics. Although ignition occurs during the high-temperature reaction phase, the low-temperature reaction process and the transition from low to high temperature are also very important for the ignition process of the mixed fuel. Considering that CH_2O is a representative product of the low-temperature reaction process, the mixed fuel reaction path under conditions of an initial temperature of 800 K, pressure of 50 bar, equivalence ratio of 1, and n-heptane molar fraction of 0.1 is shown in Figure 19 at the moment when the CH_2O generation rate reaches its maximum. At this moment, the reaction of NH_3 is very slow and has almost no contribution to the CH_2O generation process. Therefore, the NH_3 reaction path is simplified in the mixed fuel reaction path. From the figure, it can be seen that OH and O_2 participate in the main cracking process of n-heptane, and the change in NH3 molar fraction has a small effect on the main cracking process of n-heptane. It slightly reduces the process of C7H16 → C7H15-2 → C7H15O2 and slightly increases the processes C7H15O2 → C7H14O2H and C7H14O2HO2 → C7KET21 → CH2O. There is a cross-reaction between CH4 and NH3 (R111: CH4 + NH2 → CH3 + NH3). CH_4 has two main decomposition pathways in the process of generating CH_3, both of which require OH and NH_2 participation. As the NH_3 molar fraction increases, the reaction path involving OH gradually weakens, while the path involving NH_2 gradually strengthens. At an NH_3 molar fraction of 0.3, the reaction strength involving NH_2 is 45%, surpassing that of the reaction involving OH, because the increase in NH_3 concentration directly leads to an increase in NH_2 molar fraction. The reaction processes CH3 → CH3O → CH2O and HCO → CO are less affected by the NH_3 molar fraction. Overall, in the low-temperature reaction phase, the dehydrogenation reaction of CH_4 is more affected by NH_2, and as the

NH_3 molar fraction increases, the reaction strength of NH_2 with CH_4 gradually surpasses that of OH with CH_4.

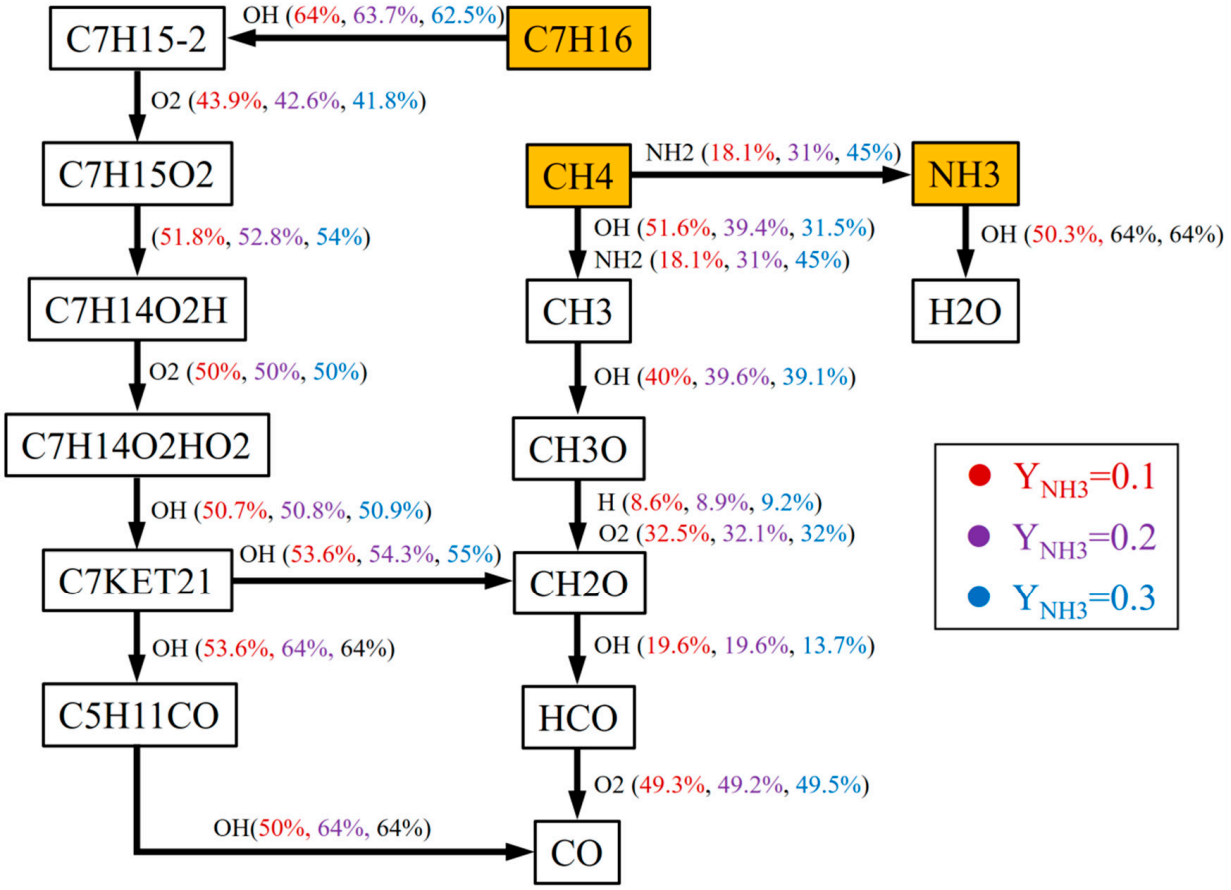


Figure 19. Reaction pathway analysis of mixed fuel at the moment of maximum CH_2O formation rate under initial conditions of 800 K, 50 bar, equivalence ratio of 1, and n-heptane molar fraction of 0.1.

At an initial temperature of 800 K, the mixed fuel undergoes a brief low-temperature reaction phase. As the temperature gradually rises, free radicals such as CH_2O and H_2O_2 in the free radical pool are rapidly consumed, and some OH-containing reactions are quickly activated. CH_4 and NH_3 are rapidly consumed, OH concentration increases instantaneously, and the temperature rises sharply, marking the end of the ignition delay phase of the mixed fuel. Under conditions of an initial temperature of 800 K, pressure of 50 bar, equivalence ratio of 1, and n-heptane molar fraction of 0.1, the mixed fuel reaction path analysis at the moment of maximum OH generation rate is shown in Figure 20. At this point, n-heptane has been completely cracked, so its reaction path is no longer listed here. Only the main reaction paths for the decomposition processes of CH_4 and NH_3 are analyzed. From Figure 20, it can be seen that most of the reaction paths require OH participation, highlighting the critical role of OH in the high-temperature reaction phase. As the NH_3 molar fraction increases, the intensity of CH_4 dehydrogenation reactions involving OH significantly decreases, while the intensity of CH_4 dehydrogenation reactions involving NH_2 increases notably. There is a cross-reaction between CH_4 and NH_3 (R111: CH4 + NH2 → CH3 + NH3), which hinders the smooth progression of the fuel oxidation process. As the NH3 molar fraction increases, the intensity of the CH3 → CH3O reaction gradually weakens, and the intensity of the CH3O → CH2O reaction involving H also gradually weakens. However, the CH3O → CH2O reaction involving OH gradually strengthens.

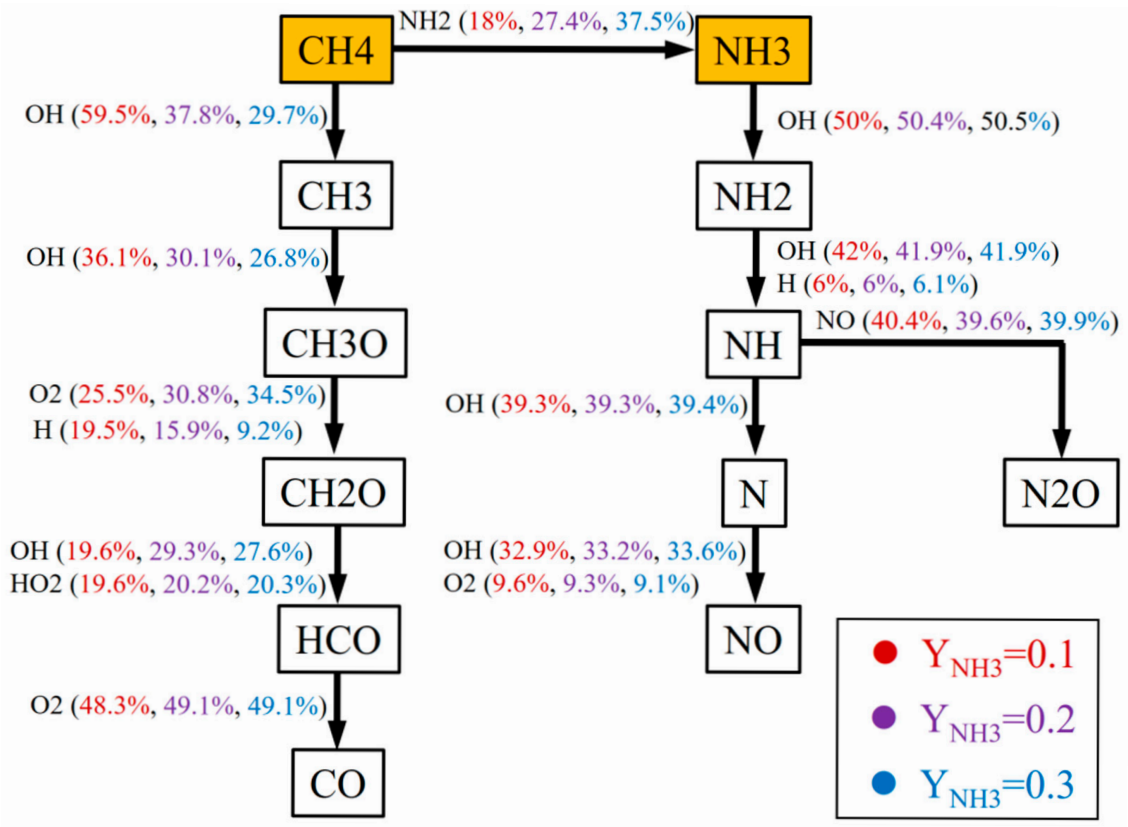


Figure 20. Reaction pathway analysis of mixed fuel at the moment of maximum OH formation rate under initial conditions of 800 K, 50 bar, equivalence ratio of 1, and n-heptane molar fraction of 0.1.

4. Conclusions

This study constructs a reaction mechanism for the n-heptane/methane/ammonia mixed fuel based on the Chemkin zero-dimensional homogeneous reactor. Some of the elementary reaction rate constants have been modified, and the ignition delay time of the simplified mechanism has been validated. The ignition delay times of pure methane, methane/ammonia mixtures, and n-heptane under high-pressure conditions were respectively verified. Using this mechanism, a chemical kinetics analysis under marine engine conditions was conducted. The specific conclusions are as follows:

(1) Using the constructed n-heptane/methane/ammonia mixed fuel chemical reaction mechanism, the effects of temperature range (800–1200 K), pressure (40–180 bar), equivalence ratio (0.5–3), and the mixing ratio of n-heptane/methane/ammonia on ignition delay time were investigated. A special trend in the ignition delay time was observed when the n-heptane/methane/ammonia mixing ratio was varied. Specifically, as the NH_3 molar fraction increased, the negative temperature coefficient phenomenon exhibited by the n-heptane/methane/ammonia mixed fuel ignition delay time became more pronounced. As the NH_3 molar fraction increased and the CH_4 molar fraction decreased, the oxygen concentration in the limited space gradually decreased. The low-activity intermediate products generated from n-C_7H_{16} cracking depend on oxygen atoms, and when O_2 concentration decreases, these products gradually accumulate under medium to low-temperature conditions, thus intensifying the negative temperature coefficient phenomenon.

(2) A sensitivity analysis of the ignition process of the mixed fuel was conducted, revealing that R49, R135, and R67 play a dominant role in promoting ignition. As the NH_3 molar fraction increases, this promoting effect gradually weakens, indicating

that the increase in NH_3 concentration delays the ignition delay time. At an initial temperature of 800 K, after the addition of ammonia fuel, it competes with other fuels for oxygen resources, leading to a slowdown in the oxidation processes of other fuels and radicals.

(3) The formation of NO mainly relies on the reactions between N and O, O_2, and OH radicals. Among these, the reaction R88 (R88: N + O2 = NO + O) has the greatest impact on the rate of production (ROP) of NO, and as the NH_3 molar fraction increases, the rate of NO production through R88 also increases. This indicates that high-temperature, oxygen-rich environments and a high NH_3 blending ratio are more likely to produce NO emissions. The formation of N_2O primarily depends on the reaction R105 (NH + NO = N2O + H) between NH and NO. As the NH_3 molar fraction increases, the rate of N_2O production through R105 also increases. The consumption of N_2O mainly relies on reactions R92 (N2O + H = N2 + OH) and R94 (N2O (+M) = N2 + O (+M)). The consumption process of N_2O is slower than its formation in R105, indicating that the consumption of N_2O is more temperature-dependent.

Author Contributions: Conceptualization, J.R., Z.S. and L.J.; Methodology, H.L.; Software, J.Z. and L.J.; Validation, J.Z.; Formal analysis, H.L.; Investigation, J.R., X.B., C.Z. and D.D.; Resources, C.Z., D.L. and J.X.; Data curation, J.R., H.L. and C.Z.; Writing—original draft, J.R.; Writing—review & editing, Z.S. and L.J.; Visualization, J.Z.; Supervision, Z.S. and D.D.; Project administration, X.B., D.L. and J.X. All authors have read and agreed to the published version of the manuscript.

Funding: This research received no external funding.

Data Availability Statement: The data presented in this study are available on reasonable request from the corresponding author. The data are not publicly available due to confidentiality requirements related to ongoing research.

Conflicts of Interest: Author Dehai Li was employed by Tianjin Linghai Weiye Technology Development Co., Ltd. Author Junpeng Xin was employed by Jinyang Automotive Technology (Tianjin) Co., Ltd. The remaining authors declare that the research was conducted in the absence of any commercial or financial relationships that could be construed as a potential conflict of interest.

References

1. Ong, B.C.; Kamarudin, S.K.; Basri, S. Direct liquid fuel cells: A review. *Int. J. Hydrogen Energy* **2017**, *42*, 10142–10157. [CrossRef]
2. Soloveichik, G.L. Liquid fuel cells. *Beilstein J. Nanotechnol.* **2014**, *5*, 1399–1418. [CrossRef] [PubMed]
3. Sherif, S.A.; Zeytinoglu, N.; Veziroğlu, T.N. Liquid hydrogen: Potential, problems, and a proposed research program. *Int. J. Hydrogen Energy* **1997**, *22*, 683–688. [CrossRef]
4. Wan, Z.; Tao, Y.; Shao, J.; Zhang, Y.; You, H. Ammonia as an effective hydrogen carrier and a clean fuel for solid oxide fuel cells. *Energy Convers. Manag.* **2021**, *228*, 113729. [CrossRef]
5. Jayabal, R. Ammonia as a potential green dual fuel in diesel engines: A review. *Process Saf. Environ. Prot.* **2024**, *188*, 1346–1354. [CrossRef]
6. Qi, Y.; Liu, W.; Liu, S.; Wang, W.; Peng, Y.; Wang, Z. A review on ammonia-hydrogen fueled internal combustion engines. *eTransportation* **2023**, *18*, 100288. [CrossRef]
7. Sun, J.; Tang, Q.; Wen, M.; Huang, L.; Liu, H.; Yao, M. Combustion characteristics and flame development of ammonia in an optical spark-ignition engine. *Fuel* **2024**, *375*, 132601. [CrossRef]
8. Zhang, Z.; Di, L.; Shi, L.; Yang, X.; Cheng, T.; Shi, C. Effect of liquid ammonia HPDI strategies on combustion characteristics and emission formation of ammonia-diesel dual-fuel heavy-duty engines. *Fuel* **2024**, *367*, 131450. [CrossRef]
9. Mathieu, O.; Petersen, E.L. Experimental and modeling study on the high-temperature oxidation of Ammonia and related NO_x chemistry. *Combust. Flame* **2015**, *162*, 554–570. [CrossRef]
10. Song, Y.; Hashemi, H.; Christensen, J.M.; Zou, C.; Marshall, P.; Glarborg, P. Ammonia oxidation at high pressure and intermediate temperatures. *Fuel* **2016**, *181*, 358–365. [CrossRef]
11. Nakamura, H.; Hasegawa, S.; Tezuka, T. Kinetic modeling of ammonia/air weak flames in a micro flow reactor with a controlled temperature profile. *Combust. Flame* **2017**, *185*, 16–27. [CrossRef]

12. Glarborg, P.; Miller, J.A.; Ruscic, B.; Klippenstein, S.J. Modeling nitrogen chemistry in combustion. *Prog. Energy Combust. Sci.* **2018**, *67*, 31–68. [CrossRef]
13. Shrestha, K.P.; Seidel, L.; Zeuch, T.; Mauss, F. Detailed Kinetic Mechanism for the Oxidation of Ammonia Including the Formation and Reduction of Nitrogen Oxides. *Energy Fuels* **2018**, *32*, 10202–10217. [CrossRef]
14. Otomo, J.; Koshi, M.; Mitsumori, T.; Iwasaki, H.; Yamada, K. Chemical kinetic modeling of ammonia oxidation with improved reaction mechanism for ammonia/air and ammonia/hydrogen/air combustion. *Int. J. Hydrogen Energy* **2018**, *43*, 3004–3014. [CrossRef]
15. Okafor, E.C.; Naito, Y.; Colson, S.; Ichikawa, A.; Kudo, T.; Hayakawa, A.; Kobayashi, H. Measurement and modelling of the laminar burning velocity of methane-ammonia-air flames at high pressures using a reduced reaction mechanism. *Combust. Flame* **2019**, *204*, 162–175. [CrossRef]
16. Mei, B.; Zhang, X.; Ma, S.; Cui, M.; Guo, H.; Cao, Z.; Li, Y. Experimental and kinetic modeling investigation on the laminar flame propagation of ammonia under oxygen enrichment and elevated pressure conditions. *Combust. Flame* **2019**, *210*, 236–246. [CrossRef]
17. Li, R.; Konnov, A.A.; He, G.; Qin, F.; Zhang, D. Chemical mechanism development and reduction for combustion of $NH_3/H_2/CH_4$ mixtures. *Fuel* **2019**, *257*, 116059. [CrossRef]
18. Stagni, A.; Arunthanayothin, S.; Maffei, L.P.; Herbinet, O.; Battin-Leclerc, F.; Faravelli, T. An experimental, theoretical and kinetic-modeling study of hydrogen sulfide pyrolysis and oxidation. *Chem. Eng. J.* **2022**, *446*, 136723. [CrossRef]
19. Han, X.; Wang, Z.; Costa, M.; Sun, Z.; He, Y.; Cen, K. Experimental and kinetic modeling study of laminar burning velocities of NH_3/air, NH_3/H_2/air, NH_3/CO/air and NH_3/CH_4/air premixed flames. *Combust. Flame* **2020**, *206*, 214–226. [CrossRef]
20. Yu, L.; Zhou, W.; Feng, Y.; Wang, W.; Zhu, J.; Qian, Y.; Lu, X. The effect of ammonia addition on the low-temperature autoignition of n-heptane: An experimental and modeling study. *Combust. Flame* **2020**, *217*, 4–11. [CrossRef]
21. Wang, Z.; Han, X.; He, Y.; Zhu, R.; Zhu, Y.; Zhou, Z.; Cen, K. Experimental and kinetic study on the laminar burning velocities of NH_3 mixing with CH_3OH and C_2H_5OH in premixed flames. *Combust. Flame* **2021**, *229*, 111392. [CrossRef]
22. Bertolino, A.; Fürst, M.; Stagni, A.; Frassoldati, A.; Pelucchi, M.; Cavallotti, C.; Faravelli, T.; Parente, A. An evolutionary, data-driven approach for mechanism optimization: Theory and application to ammonia combustion. *Combust. Flame* **2021**, *229*, 111366. [CrossRef]
23. Sun, J.; Yang, Q.; Zhao, N.; Chen, M.; Zheng, H. Numerically study of CH_4/NH_3 combustion characteristics in an industrial gas turbine combustor based on a reduced mechanism. *Fuel* **2022**, *327*, 124897. [CrossRef]
24. Liao, W.; Wang, Y.; Chu, Z.; Tao, C.; Yang, B. Chemical insights into the two-stage ignition behavior of NH_3/H_2 mixtures in an RCM. *Combust. Flame* **2023**, *256*, 112985. [CrossRef]
25. Liao, W.; Chu, Z.; Wang, Y.; Li, S.; Yang, B. An experimental and modeling study on auto-ignition of ammonia in an RCM with N_2O and H_2 addition. *Proc. Combust. Inst.* **2023**, *39*, 4377–4385. [CrossRef]
26. Xu, L.; Chang, Y.; Treacy, M.; Zhou, Y.; Jia, M.; Bai, X.-S. A skeletal chemical kinetic mechanism for ammonia/n-heptane combustion. *Fuel* **2023**, *331*, 126630. [CrossRef]
27. Wu, B.; Wang, Y.; Wang, D.; Feng, Y.; Jin, S. Generation mechanism and emission characteristics of N_2O and NO_x in ammonia-diesel dual-fuel engine. *Energy* **2023**, *284*, 129291. [CrossRef]
28. Wang, B.; Dong, S.; Jiang, Z.; Gao, W.; Wang, Z.; Li, J.; Yang, C.; Wang, Z.; Cheng, X. Development of a reduced chemical mechanism for ammonia/n-heptane blends. *Fuel* **2023**, *338*, 127358. [CrossRef]
29. Dagaut, P.; Glarborg, P.; Alzueta, M. The oxidation of hydrogen cyanide and related chemistry. *Prog. Energy Combust. Sci.* **2008**, *34*, 1–46. [CrossRef]
30. Klippenstein, S.J.; Harding, L.B.; Glarborg, P.; Miller, J.A. The role of NNH in NO formation and control. *Combust. Flame* **2011**, *158*, 774–789. [CrossRef]
31. Tian, Z.; Li, Y.; Zhang, L.; Glarborg, P.; Qi, F. An experimental and kinetic modeling study of premixed $NH_3/CH_4/O_2$/Ar flames at low pressure. *Combust. Flame* **2009**, *156*, 1413–1426. [CrossRef]
32. ANSYS, Inc. *ANSYS Help Documentation, Release 2024 R1*; ANSYS, Inc.: Canonsburg, PA, USA, 2024.
33. Rahimi, A.; Fatehifar, E.; Saray, R. Development of an optimized chemical kinetic mechanism for homogeneous charge compression ignition combustion of a fuel blend of n -heptane and natural gas using a genetic algorithm. *Proc. Inst. Mech. Eng. Part D-J. Automob. Eng.* **2010**, *224*, 1141–1159. [CrossRef]
34. Klippenstein, S.J.; Glarborg, P. Theoretical kinetics predictions for NH_2+HO_2. *Combust. Flame* **2022**, *236*, 111787. [CrossRef]
35. Glarborg, P. The $NH_3/NO_2/O_2$ system: Constraining key steps in ammonia ignition and N_2O formation. *Combust. Flame* **2023**, *257*, 112311. [CrossRef]
36. Liao, W.; Wang, Y.; Chu, Z.; Yang, B. Investigating auto-ignition characteristics and kinetic modeling of NH_3/CH_4 mixtures using an RCM. *Combust. Flame* **2024**, *260*, 113257. [CrossRef]
37. El Merhubi, H.; Kéromnès, A.; Catalano, G.; Lefort, B.; Le Moyne, L. A high pressure experimental and numerical study of methane ignition. *Fuel* **2016**, *177*, 164–172. [CrossRef]

38. Petersen, E.L.; Davidson, D.F.; Hanson, R.K. Kinetics modeling of shock-induced ignition in low-dilution CH_4/O_2 mixtures at high pressures and intermediate temperatures. *Combust. Flame* **1999**, *117*, 272–290. [CrossRef]
39. Tao, F.; Golovitchev, V.I.; Chomiak, J. Self-Ignition and Early Combustion Process of n-Heptane Sprays Under Diluted Air Conditions: Numerical Studies Based on Detailed Chemistry. *SAE Tech. Pap.* **2000**, *109*, 2837–2854. [CrossRef]
40. Adewale, C.; Reganold, J.P.; Higgins, S.; Evans, R.D.; Carpenter-Boggs, L. Agricultural carbon footprint is farm specific: Case study of two organic farms. *J. Clean. Prod.* **2019**, *229*, 795–805. [CrossRef]

Disclaimer/Publisher's Note: The statements, opinions and data contained in all publications are solely those of the individual author(s) and contributor(s) and not of MDPI and/or the editor(s). MDPI and/or the editor(s) disclaim responsibility for any injury to people or property resulting from any ideas, methods, instructions or products referred to in the content.